ELSEVIER

Journal of Alloys and Compounds 275–277 (1998) 442–446

Journal of ALLOYS AND COMPOUNDS

New anisotropic rare earth fluorides BaR_2F_8 (R=Y, Dy–Lu): growth and characterization

A.A. Kaminskii[a,*], A.V. Butashin[a], J. Hulliger[b], Ph. Egger[b], S.N. Bagayev[c], H.J. Eichler[d], J. Findeisen[d], B. Liu[d], U. Täuber[d], P. Peuser[e], S.N. Sulyanov[a]

[a]*Institute of Crystallography, Russian Academy of Sciences, Leninskii pr. 59, 117333 Moscow, Russia*
[b]*University of Berne, Dept. of Chemistry and Biochemistry, Freiestrasse 3, CH-3012 Berne, Switzerland*
[c]*Institute of Laser Physics, Russian Academy of Sciences, Siberian Division, Lavrentyev pr. 13/3, 630090 Novosibirsk, Russia*
[d]*Optical Institute, Technical University of Berlin, St. des 17. Juni 135, D-10623 Berlin, Germany*
[e]*Daimler-Benz AG, Forschung und Technik, Box 800465, D-81663 Munich, Germany*

Abstract

Polymorphism of BaR_2F_8 compounds is analyzed, and some peculiarities of the crystal growth from the melt are discussed. We report on the orthorhombic $BaLu_2F_8$ crystal with ordered structure, a new crystalline material for generating Ln^{3+} activator ions. Spectroscopic and laser characteristics of Nd^{3+}- and Er^{3+}-doped $BaLu_2F_8$ samples are discussed as representative examples. Besides, we pay special attention to monoclinic BaY_2F_8:Er^{3+} crystals, as active media for highly efficient CW 3 μm laser-diode pumped lasers. © 1998 Elsevier Science S.A.

Keywords: Rare earth fluorides; Ln^{3+}; Crystal growth

1. Introduction

Crystals of the fluoride compounds with ordered structure, which are doped with trivalent lanthanide ions (Ln^{3+}), occupy the specific position among almost three hundreds of the famous crystalline laser hosts. Being compared with the oxide laser crystals, these fluorides are less numerous, but are of significant spectral and laser potentiality due to their very wide transparency spectral range from vacuum UV to far IR, and comparably low extension of the phonon spectra ($\hbar\omega_{max}<450$ cm^{-1}) [1]. Thus at the moment, activator Ln^{3+} in these fluoride crystals are able to generate stimulated emission (SE) in the Stark-to-Stark transitions of 58 (among 69 of known) $4f^n$–$4f^n$ laser channels and three $4f^{n-1}5d^1$–$4f^n$ channels as well [2]. Let us note, that this number is almost twice the number of the $4f^n$–$4f^n$ laser channels in numerous oxide crystals with Ln^{3+} ions. In modern quantum electronics there are three preponderating kings of crystals with ordered structure among Ln^{3+}-ion doped laser fluorides, namely, tetragonal $LiRF_4$ with the scheelite structure (space group C_{4h}^6–$I4_1/a$) doped with Ce^{3+}, Pr^{3+}, Nd^{3+}, Tb^{3+}, Dy^{3+}, Ho^{3+}, Er^{3+} and Tm^{3+} ions, monoclinic BaR_2F_8 (C_{2h}^3–$C2/m$, β-$BaTm_2F_8$ structural type) doped with Pr^{3+}, Nd^{3+}, Dy^{3+}, Ho^{3+}, Er^{3+} and Tm^{3+} ions, and trigonal RF_3 compounds (D_{3d}^4–$P\bar{3}c1$) with the tysonite structure doped with Ce^{3+}, Pr^{3+}, Nd^{3+}, Dy^{3+}, Ho^{3+} and Er^{3+} ions (here R=Y and Ln). At present SE of the Ln^{3+} activator ions can be excited in $LiRF_4$, BaR_2F_8 and RF_3 host crystals in 51, 40 and 11 intermanifold transitions, respectively [2]. On the contrary, the most used oxide laser crystals $Y_3Al_5O_{12}$ and $YAlO_3$ doped with Ln^{3+}-ions generate SE only in 20 and 22 laser channels, respectively. That is why the search for new fluoride crystalline hosts with ordered structure for laser Ln^{3+}-ions seems to be of great urgency.

2. Phase relations in the BaF_2–RF_3 systems and the BaR_2F_8 crystal growth

Following our investigations on the anisotropic laser crystals with ordered structure, which form in the BaF_2–RF_3 systems [3–5], we present here growth from the melt, preliminary spectroscopic data, and laser generation of a new orthorhombic $BaLu_2F_8$:Nd^{3+} crystal and 3-μm CW laser generation of monoclinic BaY_2F_8:Er^{3+} crystal [6–9].

*Corresponding author. Fax: +7 95 1351011; e-mail: kamin@orc.ru

0925-8388/98/$19.00
PII: S0925-8388(98)00364-8

Fluoride BaR_2F_8 compounds with ordered crystal structure occur in the BaF_2–RF_3 systems with R=Y, Dy to Lu [10]. They melt (except $BaDy_2F_8$ and $BaHo_2F_8$) congruently at ≈950°C, but possess polymorphism. Typical examples of thermal behavior of the BaR_2F_8 compounds are shown in Fig. 1. Low-temperature phases β-BaR_2F_8 with R=Y, Er to Lu, which relate to the structural type of monoclinic β-$BaTm_2F_8$, undergo α↔β phase transitions somewhat below the melting points. This property appears to be the main obstacle in growing monoclinic β-BaR_2F_8 crystals of laser quality [4,5,11]. Fortunately, the majority of the BaR_2F_8 melts exhibit a considerable supercooling below their melting points, making it possible to crystallize the low temperature monoclinic phase directly omitting α–β phase transitions. According to our experience the conditions of such crystallization can be realized simply using the vertical Bridgman–Stockbarger growth technique with spontaneous seeding (see, for example, [3–5]). Our graphite furnace is designed to provide an axial thermal gradient in the crystallization area of about 70 to 100°C cm^{-1}. This gradient value supplies the melt supercooling, which permits the crystallization of the low temperature monoclinic BaR_2F_8 phase directly and to prevent undesirable crystallization of the melt. Here monoclinic BaR_2F_8 (R=Y, Ho to Yb) single crystals, which are cylindrically shaped and elongated preferably in the *c*-axis direction due to a significant extent of the growth rate anisotropy, can be grown routinely. In addition, to attain an optical homogeneity of the monoclinic crystals and to prevent cracking of the as-grown crystals, they are annealed during a few hours and cooled down slowly at a rate of ≈1°C min^{-1}. It was found too, that the solid solution ranges of the monoclinic compounds BaR_2F_8 (R=Y, Ho to Yb) are extremely narrow, and even small deviations of the melt composition from the stoichiometric (BaF_2 – 33.33 mol%, RF_3 – 66.66 mol%) makes a crystal of poor optical quality (cracking, second phase precipitation, lineage, and so on). For the present investigation we grew a series of monoclinic BaY_2F_8:Er^{3+} crystals with different dopant concentrations (C_{Er}=5–30 at.%) and crystal orientations.

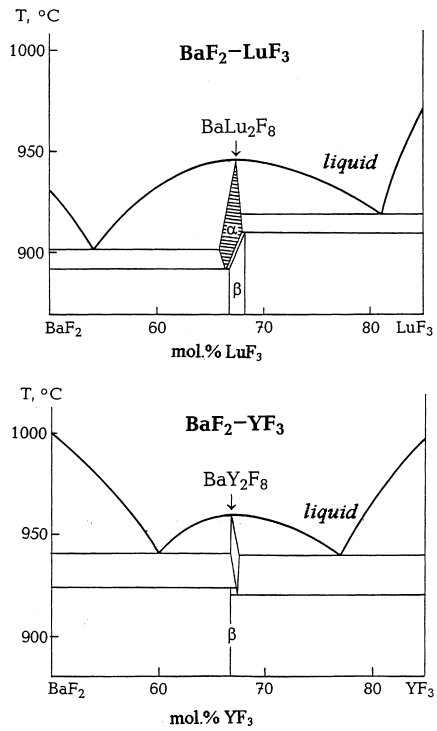

Fig. 1. Fragments of phase diagrams of the systems BaF_2–YF_3 and BaF_2–LuF_3. Phase notations: α-orthorhombic, β-monoclinic of β-$BaTm_2F_8$ type.

Based upon the similarity of the BaF_2–RF_3 phase diagram structure (R=Y, Er–Lu), the first experiments on the $BaLu_2F_8$ crystal growth were carried out by the Bridgman–Stockbarger technique using a modified KPCh-M apparatus under the above conditions. The crystallization was maintained in a static fluorinating atmosphere with a rate of ≈2 mm h^{-1}. Pure graphite was used for manufacturing the components of the growth furnace and crucibles. The loads used for growing were synthesized by melting the stoichiometric mixture of the highest purity BaF_2 and LnF_3 chemicals. They were premelted in a fluorinating atmosphere to remove traces of oxygen and moisture from the surface of the starting chemical powders. So, we found that in the thermal conditions, which were used for growing monoclinic phases, $BaLu_2F_8$ crystallizes in orthorhombic α-modification, but the crystals fail completely due to the α→β phase transition at ≈900°C. To obtain orthorhombic $BaLu_2F_8$ single crystals as well as Nd^{3+}- and Er^{3+}-ion doped samples of the acceptable dimensions (10 mm in diameter and 40 mm in length) and optical quality, we modified our graphite furnace to reduce the axial thermal gradient down to 10°C cm^{-1}, and used a quenching (cooling down at a rate≈10°C min^{-1}) of as-grown crystals. The compositions of the Er^{3+} and Nd^{3+} doped $BaLu_2F_8$ crystals have been determined by electron microprobe (CAMECA SX50). The distribution coefficients have been found to be ~0.9 for Er^{3+} and ~0.2 for Nd^{3+}.

According to the phase diagram (Fig. 1) orthorhombic $BaLu_2F_8$ is a metastable phase at room temperature. So, the information on temperature range of its stability is of great importance. In this respect, we heated polished samples of α-$BaLu_2F_8$ single crystal in pure argon for visual inspection. The α→β transition is found to begin at T_1≈350°C, resulting in the appearance of several dark stripes. At T_2≈700°C the samples turned totally opaque and single crystals were destroyed. An X-ray phase analysis indicates a complete transformation of α-$BaLu_2F_8$ into the monoclinic β-form.

3. Structure and optical spectroscopy of orthorhombic $BaLu_2F_8$ laser crystal-host

The powder diffraction pattern of the crushed $BaLu_2F_8$ crystal was obtained by a KARD-6 X-ray diffractometer

with a two-dimensional detector [12]. Reflection geometry, aperture collimation of the initial X-ray beam, and graphite monochromator (Cu Kα-emission) were used for the survey. The diffraction pattern of $BaLu_2F_8$ crystal was indexed as orthorhombic with the unit cell parameters $a=0.6904(2)$, $b=0.8094(4)$ and $c=2.1900(7)$ nm, using the DICVOL 91 program [13]. Refined X-ray parameters and density $d_{exp.}=6.94$ g cm^{-3} of the grown crystal are close to those of the ceramic samples $BaLu_2F_8$, communicated in Ref. [14]. Some basic physical characteristics of a new crystalline laser host $BaLu_2F_8$ and monoclinic BaY_2F_8 crystal (for comparison) are listed in Table 1.

The structure of the high-temperature α-$BaLu_2F_8$ phase, which was determined in Ref. [15], is orthorhombic (space group D_{2h}^{16}–*Pnma*, $Z=8$) and differs slightly from the monoclinic β-$BaTm_2F_8$ type [4]. This orthorhombic structure is a framework, which is formed by LuF_8 polyhedra linked together by sharing corners and edges (Fig. 2). It is important to note, that the cations in the structure are located in two different positions, in particular, there are two different LuF_8 polyhedra of C_1 point symmetry. The environment of Lu_1- and Lu_2-polyhedra differ noticeably, namely in the first one, the Lu–F distances range from 2.18 to 2.28 Å. The second one is strongly distorted, having seven different Lu–F distances in the range from 2.16 to 2.26 Å, and an eighth distance much longer. For this reason, one can expect to find two different activator Ln^{3+}-centers in orthorhombic $BaLu_2F_8$:Ln^{3+} crystals, whereas in the monoclinic BaR_2F_8 crystals Ln^{3+}-ions form one type of activator center.

Actually, based upon the results of preliminary spectroscopic characterization we revealed more than one activator center in the orthorhombic $BaLu_2F_8$:Er^{3+} crystal. The luminescence and absorption of this crystal were compared with those of the monoclinic BaY_2F_8:Er^{3+} laser crystal of the same activator ion concentration ($C_{Er}\approx 3$ at.%) in the resonance $^4S_{3/2}\leftrightarrow{}^4I_{15/2}$ intermanifold transition at 77 K (Fig. 3). Thus, in the luminescence spectrum of BaY_2F_8:Er^{3+} crystal with the single site for activator Er^{3+}-ions, one can find all of the 16 possible luminescence bands between the Stark levels of $^4S_{3/2}$ and $^4I_{15/2}$ states (point symmetry of the local Er^{3+} center is C_2). On the contrary, the luminescence spectrum of the $BaLu_2F_8$:Er^{3+} crystal contains many more bands, and one can attribute these bands to two different centers, both having point

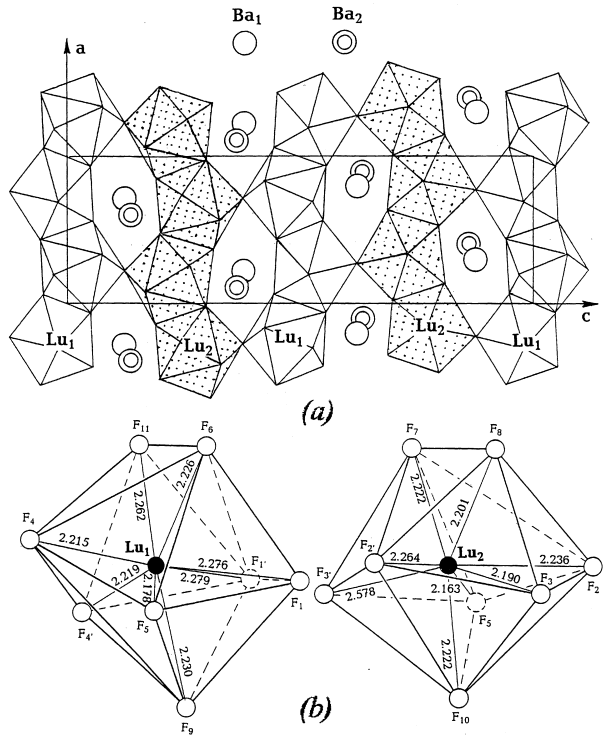

Fig. 2. (010) projection of the structure of the orthorhombic $BaLu_2F_8$ crystal (a). Lu_1- and Lu_2-polyhedra (b). Lu–F distances are given in Å.

Table 1
Some physical characteristics of anisotropic $BaLu_2F_8$ and BaY_2F_8 single crystal hosts with ordered structures

Characteristics	α-$BaLu_2F_8$	β-BaY_2F_8
Symmetry	Orthorhombic	Monoclinic
Space group	D_{2h}^{16}–*Pnma*	$C_{2h}3$–*C2/m*
Unit cell parameters (nm)	$a=0.6904(2)$	$a=0.6972$
	$b=0.8094(4)$	$b=1.0505$
	$c=2.1900(7)$	$c=0.4260$
		$\beta=99°45'$
Number of formula units	$z=8$	$z=2$
Sites symmetry for Ln^{3+} ions	C_1	C_2
Melting temperature (°C)	945	960
Density (g cm^{-3})	6.94	4.97
Linear optical classification	Biaxial	Biaxial
Optical transparent range for 1 mm thickness Plate (μm)	≈0.15 to ≈11	≈0.13 to ≈11
Thermal conductivity (W cm^{-1} K^{-1})	≈0.07	≈0.07
Hardness (Mohs scale)	4 to 5	4 to 5
Phonon spectrum expansion, $\hbar\omega_{max}$ (cm^{-1})[a]	≈400	≈420

[a] From spontaneous Raman scattering spectra.

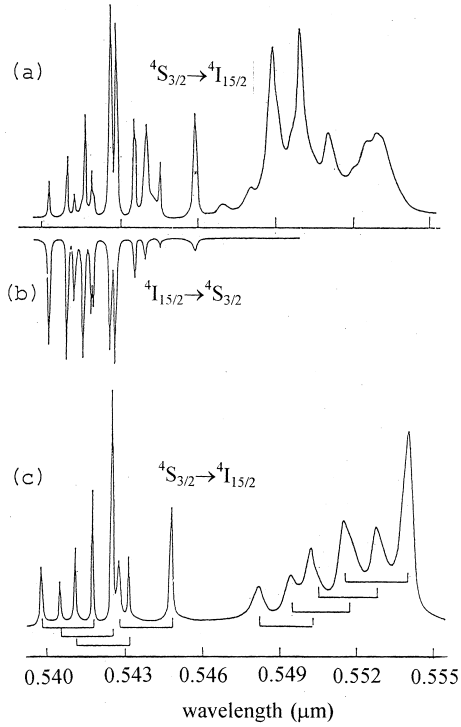

Fig. 3. Nonpolarized lumindescence and absorption spectra for the resonant intermanifold transitions $^4S_{3/2}\leftrightarrow{}^4I_{15/2}$ of Er^{3+} ions in (a) and (b) orthorhombic $BaLu_2F_8$, and (c) monoclinic BaY_2F_8 crystals at 77 K. The splitting of the metastable $^4F_{3/2}$ state in (c) is indicated by brackets.

symmetry C_1. The absorption and luminescence spectra of the $BaLu_2F_8$:Nd^{3+} crystal point to the formation of different Nd^{3+} centers in this host, too.

4. Laser action of BaR_2F_8 (R=Y and Lu) crystals doped with Nd^{3+} and Er^{3+} ions under laser-diode excitation

Quite recently we have succeeded in CW 3-μm laser action of the orthorhombic $BaLu_2F_8$:Er^{3+} crystal. Laser diode pumping was performed by means of a 1-W InGaAs diode with a wavelength between 968.5–969 nm. The results of energy spectroscopic parameter measurements of

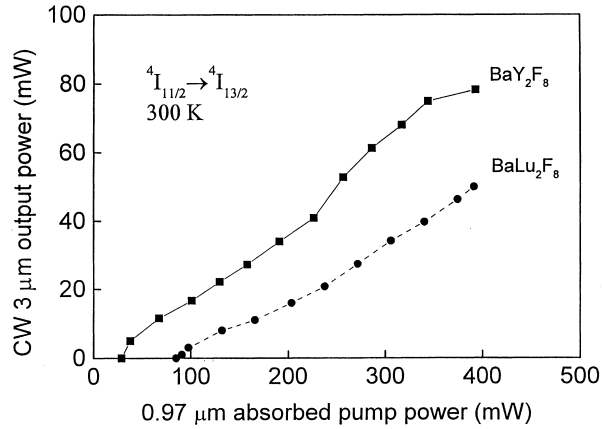

Fig. 4. Input–output characteristics of CW 3-micron lasers on the basis of anisotropic $BaLu_2F_8$ and BaY_2F_8 crystals doped with Er^{3+} ions (C_{Er}=5 at.%), pumped by a 969-nm laser diode.

single mode 3-μm CW stimulated emission of Er^{3+} ions in this crystal and in the monoclinic BaY_2F_8:Er^{3+} crystal (for comparison), are listed in Table 2 and illustrated by Fig. 4. A systematic investigation on a serious of monoclinic BaY_2F_8:Er^{3+} crystals with different dopant concentrations and orientations was carried out to optimize laser action in this 3-μm laser medium by laser-diode pumping [16]. The highest slope efficiency of 32% near the quantum defect (35%) was obtained with a 10% doped BaY_2F_8:Er^{3+} crystal with the orientation along the *b*-axis and a length of 3.5 mm.

Furthermore, we obtained room temperature single-mode CW laser operation in the $^4F_{3/2}\rightarrow{}^4I_{11/2}$ channel with GaAlAs laser diode pumping of the $BaLu_2F_8$:Nd^{3+} crystal (Table 2 and Fig. 5). To optimize laser operation it is required to grow $BaLu_2F_8$ crystals doped with Er^{3+} and Nd^{3+} ions of the optimal orientation with higher activator ion concentration and length, as well as to investigate excitation conditions thoroughly.

5. Conclusion

Thus, the growth conditions were determined for growing, and single crystals of a cubic centimeter in volume of

Table 2
Some spectroscopic and CW laser-action characteristics of Er^{3+} (C_{Er}=5 at.%) and Nd^{3+} (C_{Nd}≈0.1 at.%) ions in orthorhombic $BaLu_2F_8$ and monoclinic BaY_2F_8 crystals under laser-diode excitation at 300 K

Characteristics	$BaLu_2F_8$		BaY_2F_8
	Er^{3+}	Nd^{3+}	Er^{3+}
SE channel	$^4I_{11/2}\leftrightarrow{}^4I_{13/2}$	$^4F_{3/2}\leftrightarrow{}^4I_{11/2}$	$^4I_{11/2}\leftrightarrow{}^4I_{13/2}$
SE wavelength (μm)	≈2.795[a]	1.0483	2.7980
threshold (mW)	≈20	≈300	≈35
length of laser element (mm)	5	15	5
Luminescence lifetimes of the initial laser states (ms)	≈9	≈0.4	≈11

[a] Several lines in the range.

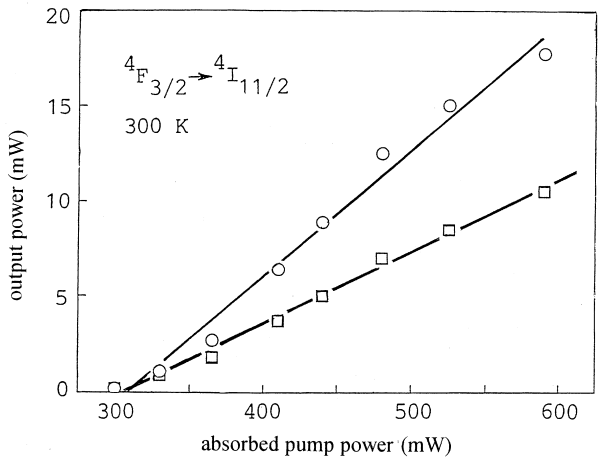

Fig. 5. Input–output characteristics of single-mode CW laser operation for a diode pumped $BaLu_2F_8:Nd^{3+}$ crystal under two different conditions: with (○) and without (□) antireflection coating on the optical faces of the laser crystal. The corresponding slope efficiencies are η=6.6% and η=3.7%, respectively.

orthorhombic $BaLu_2F_8$ fluoride are obtained from the melt for the first time. This new fluoride crystal with ordered structure is found to be a new promising crystalline host for the laser Ln^{3+} ions. Single-mode CW laser action of Er^{3+} (three micron $^4I_{11/2} \rightarrow {}^4I_{13/2}$ channel) and Nd^{3+} ions (one micron $^4F_{3/2} \rightarrow {}^4I_{11/2}$ channel) in the orthorhombic $BaLu_2F_8$ crystal-host was performed under laser diode pumping. Besides, the new 3 CW laser-diode pumped laser is created on the basis of monoclinic $BaY_2F_8:Er^{3+}$ crystals with the slope efficiency up to 32% near the quantum defect.

Acknowledgements

This work was financialy supported by DFG/RFFI (grant No. 436 RUS 113/115 (R)) and CEEC/NIS Swiss NF (grant No. 7SUPJO48393). The Russian authors acknowledge partial financial support from the Russian Foundation for Basic Research, as well as from Government Scientific Programs ''Fundamental Metrology'' and ''Optics. Laser Physics''. All the authors also note, that the investigations progressed considerably due to cooperation with Joint Open Laboratory for Laser Crystals and Precise Laser Systems.

References

[1] A.A. Kaminskii, Phys. Status Sol. (a) 148 (1995) 9.
[2] A.A. Kaminskii, Crystalline Lasers: Physical Processes and Operating Schemes, CRC Press, Boca Raton, NY, 1996, p. 561.
[3] A.A. Kaminskii, B.P. Sobolev, S.E. Sarkisov, Izv. AN SSSR, ser. Neorgan. Materialy 17 (1982) 1121.
[4] A.A. Kaminskii, B.P. Sobolev, S.E. Sarkisov, et al., Iz. AN SSSR, ser. Neorgan. Materialy 18 (1982) 482.
[5] A.A. Kaminskii, A.V. Butashin, V.S. Mironov, et al., Phys. Status Sol. (b) 194 (1996) 319.
[6] A.A. Kaminskii, A.V. Butashin, Docklady Acad. Nauk 151 (1996) 489.
[7] A.A. Kaminskii, A.V. Butashin, S.N. Bagaev, Kvantovaya Elektron. 26 (1996) 773.
[8] A.A. Kaminskii, A.V. Butashin, Phys. Status Sol. (a) 157 (1996) K29.
[9] A.A. Kaminskii, H.J. Eichler, D. Grebe, et al., Phys. Status Sol. (a) 158 (1996) K31.
[10] B.P. Sobolev, N.L. Tkachenko, J. Less-Common Metals 85 (1982) 155.
[11] L.H. Guilbert, J.Y. Gesland, A. Bulou, R. Retoux, Mater. Res. Bull. 28 (1993) 923.
[12] S.N. Sulyanov, A.N. Popov, D.M. Kheiker, J. Appl. Crystallogr. 27 (1994) 934.
[13] A. Boultif, D. Louer, J. Appl. Crystallogr. 24 (1991) 987.
[14] O. Greis, P. Stede, M. Kieser, Z. Anorg. Allg. Chem. 477 (1981) 133.
[15] M.I. Sirota, B.V. Bukvetskii, V.I. Simonov, Kristallografiya 20 (1975) 642.
[16] H.J. Eichler, J. Findeisen, B. Liu, A.A. Kaminskii, A.V. Butashin, P. Peuser, IEEE J. Selected Topics Quant. Electron. 3 (1997) 90.